MNRAS **000**, 1–8 (2018) Preprint 22 July 2018 Compiled using MNRAS LATEX style file v3.0

NOEMA Reveals Gas Reservoirs in a QSO Triplet

E. P. Farina,[1⋆] R. Decarli,[2] and M. Fumagalli.[3,4]

[1] *Department of Physics, Broida Hall, University of California, Santa Barbara, CA 93106–9530, USA*
[2] *Osservatorio di Astrofisica e Scienza dello Spazio di Bologna, via Gobetti 93/3, I–40129, Bologna, Italy*
[3] *Institute for Computational Cosmology, Durham University, South Road, Durham DH1 3LE, UK*
[4] *Centre for Extragalactic Astronomy, Durham University, South Road, Durham DH1 3LE, UK*

Accepted XXX. Received YYY; in original form ZZZ

ABSTRACT

QSOs are rare: less than $\sim$100 deg^{-2} at $m_i \lesssim 21$ mag. The discovery of pairs or even triplets of QSOs in clear excess with respect to simple clustering predictions suggests that, in these systems, galaxy interactions are responsible for triggering large gaseous inflow toward galaxy centres, consequently igniting the nuclear activity. We test this scenario by studying dynamics in a QSO triplet, QQQ J1519+0627 at $z\sim1.51$. In order to precisely pin down the line–of–sight relative velocity of the three host galaxies, we target their molecular gas reservoirs using *NOEMA* at 3 mm band. We detected the CO (2–1) emission from all three objects with fluxes of 0.3–0.4 Jy km s^{-1}, corresponding to CO (2–1) luminosities of the order of 10^{10}–10^{11} K km s^{-1} pc^2. These are among the faintest non–lensed type 1 QSOs detected so far in CO. We observe velocity differences between the three hosts of $<$300 km s^{-1}, confirming that the three QSOs are embedded in a halo with mass $\sim10^{12}$ h^{-1} M$_\odot$. This halo mass is comparable to the one of low–dispersion, compact groups of interacting galaxies observed in the local Universe. We gauge the molecular gas content using standard conversions. The amount of gas available for star formation, together with the dynamical description of the triplet, suggests that the system may evolve into a massive "red–and–dead" galaxy by the present age.

Key words: QSOs: general

1 INTRODUCTION

QSOs are among the most luminous astrophysical objects. As such, they have been used as probes of structure formation up to the reionization epoch (e.g., Hennawi et al. 2006, 2010; Shen et al. 2010, 2013; Eftekharzadeh et al. 2015, 2017; McGreer et al. 2016; García-Vergara et al. 2017; Farina et al. 2017; Decarli et al. 2017).

The QSO activity is due to accretion onto supermassive black holes (SMBH, e.g., Salpeter 1964; Lynden-Bell 1969; Soltan 1982) residing at the centre of massive galaxies (e.g., Kormendy & Richstone 1995; Ferrarese & Ford 2005; Decarli et al. 2007; Kormendy & Ho 2013). In the current hierarchical paradigm of galaxy formation (e.g., White & Rees 1978), these massive galaxies undergo multiple merger events during their lifetime. Tidal interactions are able to trigger intense bursts of star formation and to funnel huge amount of gas in the nuclear region, flaring up the activity of the central SMBH (e.g., Springel, Di Matteo, & Hernquist 2005; Di Matteo, Springel, & Hernquist 2005). Radiative and/or mechanical feedback from the active nucleus is then believed to quench star formation, transforming the host galaxies into massive, *red–and–dead* elliptical galaxies that typically resides in a rich group or in a cluster (e.g., Shankar, Weinberg, & Miralda-Escudé 2009; Strazzullo et al. 2010; Alexander & Hickox 2012). The analysis of large scale clustering properties of QSOs revealed that, at intermediate redshifts, they occupy dark matter haloes with $M_{halo}\simeq10^{12.5}$ M$_\odot$ (e.g., Porciani, Magliocchetti, & Norberg 2004; Croom et al. 2005; Myers et al. 2007; Farina, Falomo, & Treves 2011; White et al. 2012; Eftekharzadeh et al. 2015; Rodríguez-Torres et al. 2017), a regime where galaxies appear to be most efficient in forming stars (e.g., Moster et al. 2010; Behroozi, Conroy, & Wechsler 2010) and the frequency of mergers is higher (e.g., Lacey & Cole 1993). This picture justifies the observed enhancement of the number of QSO pairs at relatively small ($\lesssim$1 Mpc) separations with respect to the expectation from large scale clustering (e.g., Djorgovski 1991; Hennawi et al. 2006, 2010; Kayo & Oguri 2012; Myers et al. 2008; Eftekharzadeh et al. 2017).

⋆ E-mail: emanuele.paolo.farina@gmail.com

Systems of 3–4 faint (and thus, relatively common) AGN have been reported in the literature (e.g., Hennawi et al. 2015; Arrigoni Battaia et al. 2018). Remarkably, in the last decade three triplets of close, physically associated, bright QSOs have been discovered: QQQ J1432−0106 (z=2.08, Djorgovski et al. 2007), QQQ J1519+0627 (z=1.51, Farina et al. 2013), and 2RXS J150158.6+691029 (z=1.13, Assef et al. 2018). These systems represent a striking deviation from the extrapolation of the large–scale two–point correlation function, thus strengthening the evidence for a small–scale enhancement of QSO clustering.

The evolution of these QSO triplets critically depends on the relative kinematics and separations of the host galaxies, on their gaseous reservoirs (which set the potential for future star formation), and on the impact of AGN feedback. Observations of molecular gas provide important constraints on the kinematics of the galaxies, and on the mass and excitation of their interstellar medium (see Carilli & Walter 2013 for a review). At high redshift, molecular gas is traced by carbon monoxide rotovibrational lines (CO; see Carilli & Walter 2013). CO has been detected in several QSO host galaxies even at the earliest cosmic times (z>4, e.g., Carilli et al. 2002; Walter et al. 2003; Wang et al. 2011a,b; Venemans et al. 2017). At the epoch of the peak of QSO activity (z∼2–3) only few dozens of systems has been investigated, mostly preselected to be far-infrared bright (e.g., Coppin et al. 2008; Simpson et al. 2012) or lensed (e.g., Riechers et al. 2011; Tuan-Anh et al. 2017). These QSOs show the presence of massive (a few 10^{10} $M_\odot$) and compact (less than a few kiloparsecs) gas reservoirs (e.g., Carilli & Walter 2013). In this paper we present sensitive observations with the NOrthern Extended Millimeter Array (*NOEMA*) targeting the QSO triplet QQQ J1519+0627. These data allow us to probe the dynamics of the system and the amount of cold gas available for the star formation activity in the hosts, thus probing the evolutionary status of these QSOs in their pathway to become today's massive elliptical galaxies.

Throughout this paper, we assume a concordance cosmology with H_0=70 km s^{-1} Mpc^{-1}, Ω_m=0.3, and Ω_Λ=0.7. In this cosmology, at z=1.51 the Universe is 4.173 Gyr old, and an angular scale θ=1″ corresponds to a proper transverse separation of 8.5 kpc. All the quoted magnitudes are expressed in the AB standard photometric system (Oke 1974; Oke & Gunn 1983).

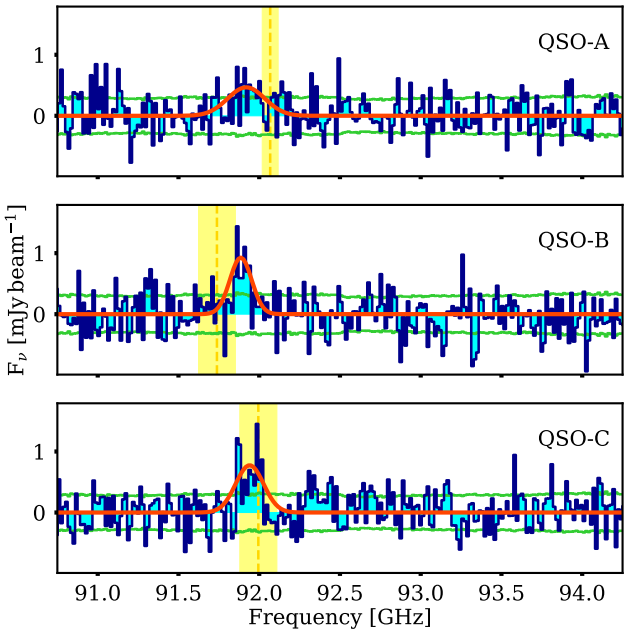

Figure 1. *NOEMA* spectra at 3 mm observed wavelengths extracted at the optical position of the three QSOs in QQQ J1519+0627 (blue solid line). The best fit of the detected CO (2–1) lines are showed as red solid lines. The expected frequencies of the CO (2–1) emission lines, calculated from the Mg II redshift of the QSOs (Farina et al. 2013), are marked with dashed orange lines, with 1σ uncertainties highlighted in yellow. The green lines show the ±1σ noise levels.

2 OBSERVATIONS AND DATA REDUCTION

We observed the CO(2-1) line in QQQ J1519+0627 during Summer 2016 (program ID: S16BQ) and Summer 2017 (program ID: S17BL). The observations were centered at R.A.=15:19:46.554 Dec=+06:27:52.240 (J2000.0). At z=1.51, the line is shifted to 91.85 GHz (3 mm). At this frequency, the full width at half power of the *NOEMA* beam is 54.″8. The 2016 data were acquired with 5-7 antennas in compact array configuration, with typical precipitable water vapour of 5–15 mm, and system temperatures of 85–150 K. The 2017 observations were carried out with 8 antennas in compact ('D') configuration, with typical precipitable water vapour of 1–5 mm and system temperatures of 55–80 K. The bright QSOs 3C454.3 and 3C273 were used for the bandpass calibration; MWC349 was used for the absolute gain calibration. The QSOs 1546+027 and 1502+106 were targeted for phase and amplitude calibration. We used clic from the GILDAS software suite to calibrate our WideX observations. After calibration and flagging, the combined tracks resulted in 18,128 visibilities, corresponding to 10.8 hr on-source (7-antennas equivalent). We imaged the cube using mapping with natural weighting, resulting in a synthesized beam of 4.″6×3.″5 (PA=9.9°). The final rms is 0.261 mJy beam^{-1} per 50 km s^{-1}, or 18.1 μJy beam^{-1} in the collapsed 3mm continuum.

3 DETECTION OF MOLECULAR GAS IN THREE QSO HOST–GALAXIES

In Figure 1 we show the *NOEMA* 3 mm spectra extracted at the optical position of the three QSOs, corrected for the primary beam attenuation at the respective positions of the three QSOs. Emission lines are clearly detected for QSO–B and QSO–C, and marginally for QSO–A. These detections are confirmed in the map presented in the left panel of Figure 2, where we collapsed the cube over channels where lines are detected. Channels not belonging to emission lines were collapsed to create a far–infrared continuum map (Right Panel of Figure 2).

We used our own Metropolis Monte Carlo Markov Chain routine (see Decarli et al. 2018 for details) to fit the spectra, assuming a Gaussian shape for the emission

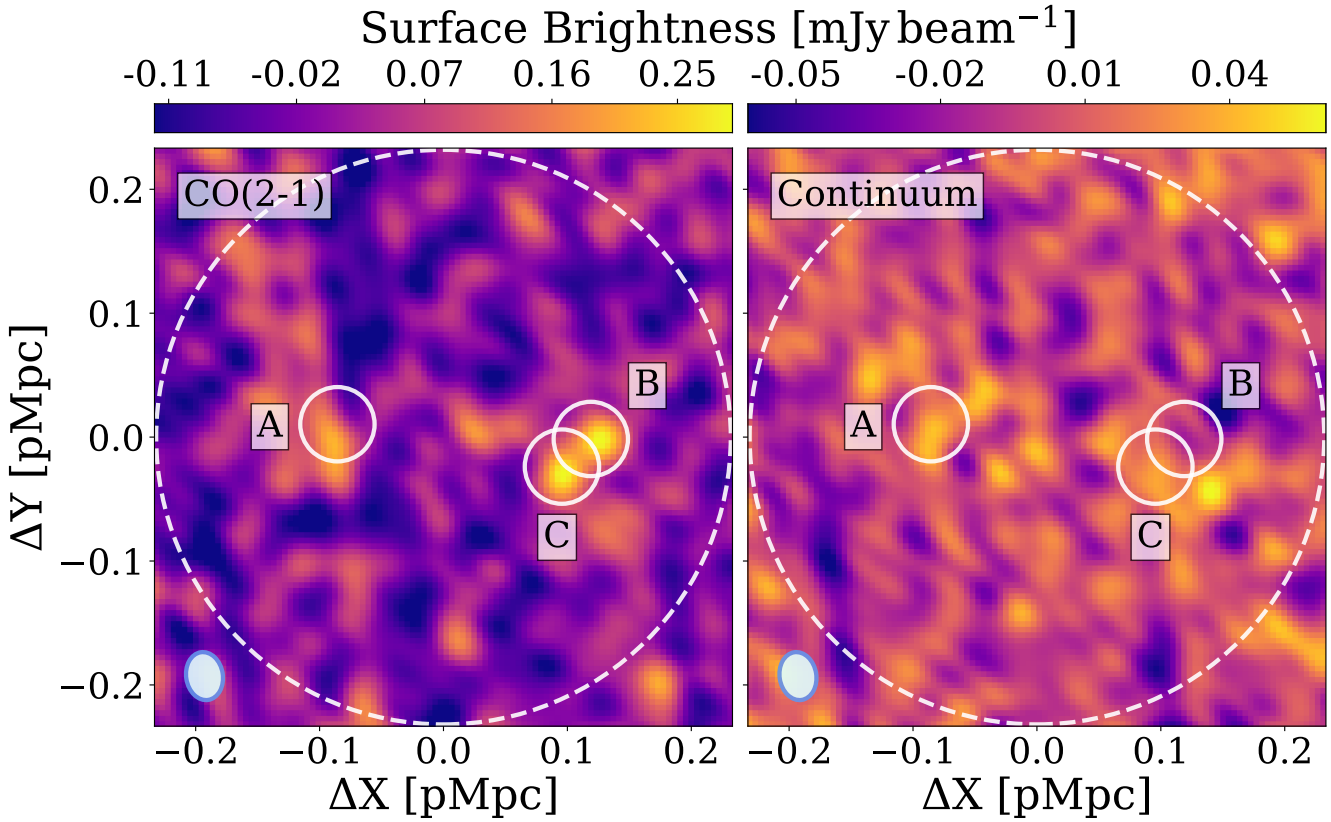

Figure 2. *NOEMA* maps of the QSO triplet QQQ J1519+0627. The white circles in each panel mark the optical position of the QSOs (labels follow the nomenclature assigned by Farina et al. 2013). The size of the beam is 4.″6×3.″5 with PA=9.9° and is showed in the bottom left corner of each panel. The big dashed circle indicates the size of the primary beam (FWHP∼54.″8). *Left* — Map of the CO (2–1) line emission integrated over a window of 1200 km s^{-1} centered at the expected position of the CO (2–1) line at the average redshift derived from the broad Mg II QSO emission lines (z=1.51, Farina et al. 2013). *Right* — Far–infrared continuum emission obtained collapsing the frequency range free from line emission. No emission is observed down to a 5 σ limit of 90.7 μJy beam^{-1}.

lines. In Table 1 we list the outcome of the fitting procedure, where inferred quantities and their uncertainties are the median and the 14%–86% quartiles of the posterior distributions. Under the assumption that these are CO (2–1) emission lines, we can derive the systemic redshifts of the host galaxies. For QSO–A, QSO–B, and QSO–C we obtain $z_{\rm CO,A}$=1.50804$^{+0.00013}_{-0.00012}$, $z_{\rm CO,B}$=1.50896$^{+0.00030}_{-0.00028}$, and $z_{\rm CO,C}$=1.50747$^{+0.00022}_{-0.00022}$, respectively. These redshifts appear to be displaced from those derived from Mg II (marked as vertical dashed lines in Figure 1). The relative velocity difference between the peak of the Mg II and of the CO (2–1) ($\Delta V_{\rm MgII\text{-}CO}$) can be quantified as:

$$\Delta V_{\rm MgII\text{-}CO} = c\,\frac{z_{\rm MgII} - z_{\rm CO}}{1+z_{\rm CO}}, \qquad (1)$$

where c is the speed of light, and a positive value of $\Delta V_{\rm MgII\text{-}CO}$ indicates that the Mg II line is blueshifted with respect to the CO (2–1) line. The observed velocity shifts, ranging from −480 to +180 km s^{-1}, are not surprising. In $z\lesssim$1 QSOs, the Mg II line has a broad distribution in velocity differences with respect to the [O III] emission line (considered as a good proxy of the systemic redshift at low redshift) with a median shift of −97 km s^{-1} and a dispersion of 269 km s^{-1} (e.g., Richards et al. 2002; Bonning, Shields, & Salviander 2007; Hewett & Wild 2010). We thus consider the detected emission as CO (2–1) associated to the hosts of the three QSOs in the triplet. The lines have FWHMs between ∼350 km s^{-1} and ∼650 km s^{-1} and velocity–integrated fluxes between ∼0.30 Jy km s^{-1} and ∼0.40 Jy km s^{-1}. These correspond to luminosities of the CO (2–1) lines of 9–10 ×10^9 K km s^{-1} pc^2. The CO excitation ladder of QSOs typically resambles those of nearby starburst galaxies such as M82 (e.g., Carilli & Walter 2013). In this highly excited environment CO is often thermalized up to $J_{\rm up}>4$. The conversion between CO (2–1) and CO (1–0) luminosities is thus robust and of order of unity. Assuming $L'_{\rm CO(2\text{-}1)}/L'_{\rm CO(1\text{-}0)}$=0.99 (see Table 2 in Carilli & Walter 2013) we obtain CO (1–0) luminosities of $L'_{\rm CO(1\text{-}0),A}=(9.3^{+2.0}_{-2.0})\times10^9$ K km s^{-1} pc^2, $L'_{\rm CO(1\text{-}0),B}=(10.7^{+1.7}_{-1.7})\times10^9$ K km s^{-1} pc^2, and $L'_{\rm CO(1\text{-}0),C}=(11.5^{+1.6}_{-1.6})\times10^9$ K km s^{-1} pc^2, for QSO–A, QSO–B, and QSO–C, respectively. Considering the CO–to–molecular gas mass conversion factor commonly used for QSO host galaxies, $\alpha_{\rm CO}$=0.8 M$_\odot$ (km s^{-1} pc^2)$^{-1}$ (Carilli & Walter 2013; Bolatto, Wolfire, & Leroy 2013), these values translate into H_2 masses of: 7.4×10^9 M$_\odot$, 8.6×10^9 M$_\odot$, and 9.2×10^9 M$_\odot$, for QSO–A, QSO–B, and QSO–C, respectively (see Table 1). If we adopt a value

Table 1. Parameters of the lines detected at the location of the host galaxies in the QSO triplet QQQ J1519+0627 (see Figure 1). The fitting procedure and the error estimates are summarised in section 3. (1) Central frequency. (2) Line full width at half maximum. (3) Velocity integrated flux. (4) CO redshift. (5) CO (2–1) luminosity. (6) CO (1–0) luminosity calculated assuming $L'_{\rm CO(2\text{-}1)}/L'_{\rm CO(1\text{-}0)}$=0.99. (7) Molecular gas mass derived assuming $\alpha_{\rm CO}$=0.8 $M_\odot$ (km s^{-1} pc^2)$^{-1}$. (8) Relative velocity shift between Mg II and CO (2–1).

Quantity	Units	QSO–A	QSO–B	QSO–C
(1) Peak	(GHz)	$91.920^{+0.008}_{-0.007}$	$91.886^{+0.018}_{-0.017}$	$91.941^{+0.013}_{-0.014}$
(2) FWHM	(km s^{-1})	627^{+159}_{-157}	366^{+78}_{-62}	468^{+60}_{-56}
(3) Flux	(Jy km s^{-1})	$0.31^{+0.07}_{-0.07}$	$0.36^{+0.06}_{-0.06}$	$0.39^{+0.06}_{-0.06}$
(4) z		$1.50804^{+0.00013}_{-0.00012}$	$1.50896^{+0.00030}_{-0.00028}$	$1.50747^{+0.00022}_{-0.00022}$
(5) $L'_{\rm CO(2\text{-}1)}$	(10^9 K km s^{-1} pc^2)	$9.2^{+2.0}_{-2.0}$	$10.6^{+1.7}_{-1.7}$	$11.4^{+1.6}_{-1.6}$
(6) $L'_{\rm CO(1\text{-}0)}$	(10^9 K km s^{-1} pc^2)	$9.3^{+2.0}_{-2.0}$	$10.7^{+1.7}_{-1.7}$	$11.5^{+1.6}_{-1.6}$
(7) $M_{\rm H_2}$	(10^9 $M_\odot$)	7.4	8.6	9.2
(8) $\Delta V_{\rm MgII\ -\ CO}$	(km s^{-1})	−480±120	+480±360	−180±360

of $\alpha_{\rm CO}$=3.6 $M_\odot$ (km s^{-1} pc^2)$^{-1}$, typical of the Milky Way disk, the implied H_2 masses are 4.5 times larger.

4 DISCUSSION

In the previous section we presented the detection of the CO (2–1) emission lines rising from all the QSO host galaxies in the triplet QQQ J1519+0627. In the following, we estimate the likelihood to find such an overdensity of CO emitters given expectations from the field (subsection 4.1), we investigate the dynamics of the system (subsection 4.2), and we put the detections in the context of the general properties of QSOs detected in CO (subsection 4.3).

4.1 An overdensity of CO emitters

The presence of three CO (2–1) emitters in the same (small) cosmological volume represents a clear excess with respect to the field, in qualitative agreement with our selection of a QSO overdensity. We quantify the strength of such fluctuation by comparing with available (although coarse) constraints on the CO luminosity functions at these redshifts (Walter et al. 2014; Decarli et al. 2016) and with expectations from semi–analytic models by Popping et al. (2016). Assuming to integrate over a 500 km s^{-1} line, our observations reached a 3 σ flux limit of $F_{3\sigma}$=0.14 Jy km s^{-1}. This translates into a 3 σ luminosity limit for a z=1.51 CO (2–1) line of $L'_{\rm CO(2\text{-}1),3\sigma}$=4.1×10^9 K km s^{-1} pc^2, i.e. we reached the knee of the luminosity function (with $L'^{\star}_{\rm CO(2\text{-}1)}$∼10$^{9.6}$ K km s^{-1} pc^2 at z∼1.51, Popping et al. 2016). The expected number density of CO (2–1) lines down to this luminosity limit is ∼1.1×10^{-3} cMpc^{-3}. If we consider the *NOEMA* primary beam (FWHP∼54.″8, or 1.16 cMpc at z=1.51) and the WideX frequency coverage (from 90.706 to 94.294 GHz, corresponding to the redshift interval 1.44<z<1.54 for the CO (2–1) line), the cylindrical volume probed by our data is 196 cMpc^3. Hence, ∼0.2 CO (2–1) emitters would be expected *in the whole datacube*. By considering the proximity in redshift space of the three QSOs (thus limiting the volume to a slice of ±500 km s^{-1} around the triplet redshift) the number of expected sources drops to ∼0.02. In other words, the detection of three such close CO (2–1) emitters represents a deviation of a factor ∼150 from the background.

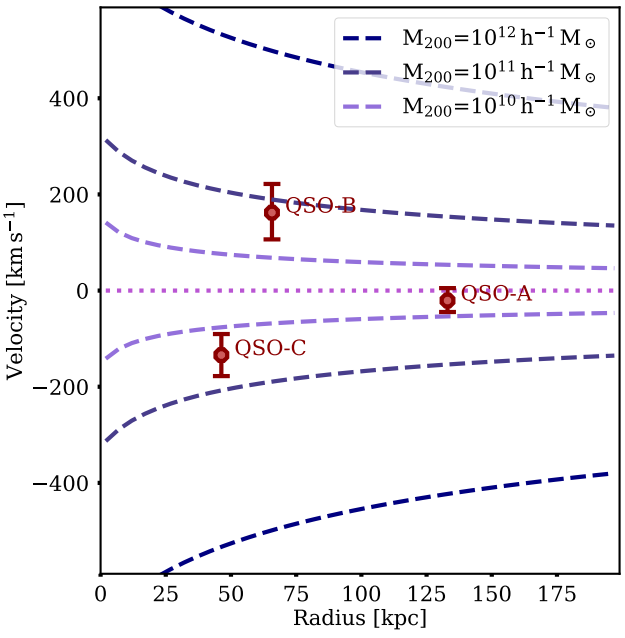

Figure 3. Velocity and position of the three QSO host galaxies relative to the centre of the system (as defined in subsection 4.2, brown points). The system is well encompassed within a velocity difference of ∼300 km s^{-1} and a radius of ∼150 kpc. The different blue dashed lines denote the escape velocity from dark matter haloes with masses M_{200}=10^{10}, 10^{11}, and 10^{12} h^{-1} $M_\odot$. We note that no projection corrections have been applyed to the velocity and to the position of the QSOs. These corrections, are expected to be on the order of a factor ∼3–4 (e.g., Limber & Mathews 1960; Farina, Falomo, & Treves 2011), implying that a correspondingly larger mass is necessary to keep the system bound.

4.2 The dynamical mass of the system

The accurate systemic redshifts derived from the CO (2–1) lines open the possibility of a precise study of the relative dynamics of the three host galaxies. The new CO (2–1) observations presented here significantly reduce the spread in line–of–sight velocity differences between the galaxies, from $\Delta V{\sim}1100\,\mathrm{km\,s^{-1}}$, as calculated by Farina et al. (2013) on the basis of the Mg II lines, to $\Delta V{\sim}300\,\mathrm{km\,s^{-1}}$ derived from the CO (2–1) lines. To assess if these host galaxies are indeed bound within the same cosmic structure, we compute the escape velocity ($V_{\rm Esc}$) of a typical dark matter halo hosting an intermediate redshift QSO. For a virialized halo with a given density profile $\rho\,(r)$, the escape velocity as a function of radius (r) can be simply expressed as:

$$V_{\rm Esc} = \sqrt{2\,|\phi\,(r)|}, \tag{2}$$

where the potential ($\phi\,(r)$) is:

$$\phi\,(r) = -\frac{\rm G}{r}\int_0^r 4\pi\rho\,(r')\,r'^2 dr' - {\rm G}\int_r^\infty 4\pi\rho\,(r')\,r' dr' \tag{3}$$

Hereafter, we will assume a NFW (Navarro, Frenk, & White 1997) density profile and the concentration–mass relation presented in Dutton & Macciò (2014)[1]. As barycentre of the system we arbitrarily choose the CO (2–1) luminosity weighted average of the source positions and of the redshifts ($\langle$R.A.$\rangle$=15:19:46.190, $\langle$Dec.$\rangle$=+06:27:51.03, and $\langle z\rangle$=1.50814). Figure 3 compares the velocity difference between the QSOs and the escape velocities calculated for halo with masses $\mathrm{M_{200}}{=}10^{10}$, 10^{11}, and $10^{12}\,\mathrm{h^{-1}\,M_\odot}$. The three host galaxies appear to lie within the escape velocity of a dark matter haloes of $\sim10^{11}\,\mathrm{h^{-1}\,M_\odot}$. Barring projection effects, this is more than an order of magnitude smaller than the characteristic halo mass of a single $z{\sim}1.5$ QSO ($\sim6{\times}10^{12}\,\mathrm{h^{-1}\,M_\odot}$, see e.g., Laurent et al. 2017), suggesting that the QSOs belong to the same halo. Using the host galaxies to probe the halo potential well (e.g., Limber & Mathews 1960), we derive a rough estimate of the virial mass of the system. Albeit based only on three galaxies, we infer the line–of–sight velocity dispersion: $\sigma_{\rm LOS}{\sim}76\,\mathrm{km\,s^{-1}}$. From this, considering the empirical relation between $\sigma_{\rm LOS}$ and virial radius observed in low redshift clusters by Girardi et al. (1998), we infer a virial mass of $\sim9.8{\times}10^{11}\,\mathrm{h^{-1}\,M_\odot}$.

We should be cautious about using the face value of the virial mass. This is indeed derived from measurement of only three galaxies and, most importantly, under the assumption that the system is in, or near to, the dynamical equilibrium. However, it is intriguing that our measurement suggests that QQQ J1519+0627 is tracing a small group a galaxies. Indeed, in these kind of environments, the effective cross section of galaxy interactions increases (e.g., Aarseth & Fall 1980), making mergers of gas rich galaxies more effective in triggering the activity the central supermassive black holes and thus increasing the chance of observing close pairs or triplet of QSOs (e.g., Hopkins et al. 2008).

[1] We note that the Planck cosmology (Planck Collaboration et al. 2014) used in Dutton & Macciò (2014) is slightly different from the one considered in this paper. However, effects of this discrepancy are negligible in the context of our calculations.

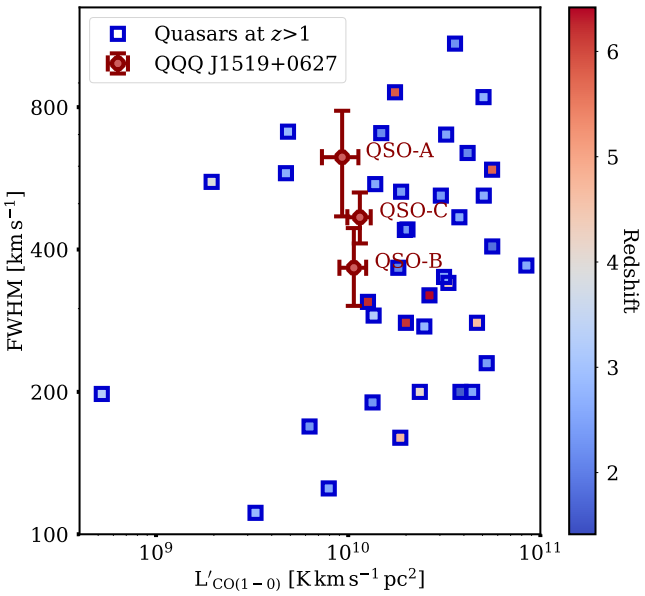

Figure 4. The CO line width versus CO luminosity. Blue squares show the location of *isolated* QSOs at $z{>}1$ from the litterature. The gradient from blue to red is representative of the object redshifts. The three CO detection associated with QQQ J1519+0627 are plotted as brown points.

4.3 Comparison with the literature

In Figure 4 we show the distribution in the $L'_{\rm CO(1\text{-}0)}$–FWHM plane of a sample of $z{>}1$ QSOs detected in CO (1–0), CO (2–1), and CO (3–2) collected from the literature[2]. We limited the comparison to these low–J transitions to minimize uncertainties due to the unconstrained CO excitation ladder for these QSOs. Considering that the CO luminosity is related to the H_2 content and FWHM of the line to the dynamical mass of a galaxy, this plane can be seen as a representation of the molecular gas fraction for QSO hosts. The three QSOs studied here show lower $L'_{\rm CO(1\text{-}0)}$ values for their FWHM than most of other QSOs reported so far in the literature. This is suggestive for a low molecular gas fraction for these objects. However, most of the QSOs detected in CO at intermediate redshift in the past decades have been lensed or pre–selected to be FIR–bright. This introduces an observational bias that skews the distribution towards high CO luminosities. The lack of CO observations in the literature in

[2] Data are from: Barvainis et al. (1998); Frayer et al. (1998); Guilloteau et al. (1999); Planesas et al. (1999); Carilli et al. (2002); Walter et al. (2003, 2004); Hainline et al. (2004); Willott, Martínez-Sansigre, & Rawlings (2007); Aravena et al. (2008); Martínez-Sansigre et al. (2009); Coppin et al. (2008, 2010); Harris et al. (2010); Wang et al. (2010, 2011a,b); Riechers et al. (2009, 2011); Riechers (2011); Simpson et al. (2012); Feruglio et al. (2014); Banerji et al. (2017), see also Carilli & Walter (2013) and references therein. Measurement for lensed objects are corrected for the magnification reported in the papers. Luminosities have been rescaled to the considered cosmology and converted to $L'_{\rm CO(1\text{-}0)}$ using the convertion factors for QSOs from Table 2 in Carilli & Walter (2013).

a statistical sample of optically–selected QSOs at intermediate redshifts hinders a self-consistent comparison between the observations presented here and the ones available in the literature.

5 SUMMARY AND CONCLUSIONS

In this paper, we present *NOEMA* 3 mm observations of QQQ J1519+0627, a triplet of QSOs located at $z\sim1.51$. These data allow us to reach a $3\,\sigma$ sensitivity for a detection of a $500\,\mathrm{km\,s^{-1}}$ line of $0.14\,\mathrm{Jy\,km\,s^{-1}}$, allowing us to search for emitters down to the knee of the CO (2–1) luminosity function at at $z\sim1.51$ ($L'_{\mathrm{CO(2\text{-}1)},3\sigma}=4.1\times10^9\,\mathrm{K\,km\,s^{-1}\,pc^2}$). The primary results of this study are:

(i) We detect the CO (2–1) line from all the three host galaxies with luminosities of $(9.2\text{–}11.4)\times10^9\,\mathrm{K\,km\,s^{-1}\,pc^2}$. This corresponds to an overdensity of a factor ~150 with respect to expectation from the blank field.

(ii) Using the molecular line as a tracer of the host galaxies' rest frame, we derive that the line–of–sight velocity spread is only $300\,\mathrm{km\,s^{-1}}$, thus confirming that they are bound in the same structure.

(iii) Under the assumption of virial equilibrium, the relative dynamics of the three host galaxies imply that the system is harboured in a halo with a virial mass of $\sim10^{12}\,\mathrm{h^{-1}\,M_\odot}$.

(iv) A comparison with detection of CO emission lines from the literature suggests that the three hosts in QQQ J1519+0627 have a lower molecular gas fraction with respect to the (biased) sample of high–z QSOs observed to date.

Based on these results, we can sketch a qualitative evolution of the system. The small dynamical mass derived from the triplet suggests that QQQ J1519+0627 is embedded in a modest–sized group of galaxies. This result is in line with the study of a sample of $z\lesssim1$ close binary QSOs performed by Green et al. (2011), who show that these systems are not tracers of cluster environments (but see, e.g., Sandrinelli et al. 2018; Onoue et al. 2018 for results obtained from QSO pairs at larger separations). We estimate that the host galaxies of the observed QSOs are of a few times $10^{11}\,\mathrm{M_\odot}$, both considering the estimated molecular gas masses alone (see Table 1), and the stellar mass derived from the black hole masses ($0.5\text{–}1.1\times10^9\,\mathrm{M_\odot}$[3], see Farina et al. 2013), assuming the evolution of the $M_{\mathrm{BH}}/M_{\mathrm{host}}$ ratio from Decarli et al. (2010). Given the low velocity dispersion of compact groups, the QSO host galaxies observed in this study are likely to merge in the following Gyr, thus leading to the formation of a massive elliptical galaxy in the local Universe.

This picture is qualitatively consistent with the study of Niemi et al. (2010). Following the evolution of galaxies in the Millennium simulation (Springel et al. 2005), they show that roughly one third of isolated elliptical galaxies has experienced at least one major merger during its evolution. At z=0, at a given stellar mass, these galaxies reside in dark matter haloes less massive than "normal" ellipticals. Future analysis of the field of QQQ J1519+0627 aimed in probing the galactic environment will provide further details on the formation and evolution of these rare systems.

[3] Specifically, from the scaling relations presented in Vestergaard & Osmer (2009) we obtain: $\mathrm{M_{BH,A}}=1.7\times10^9\,\mathrm{M_\odot}$, $\mathrm{M_{BH,B}}=0.6\times10^9\,\mathrm{M_\odot}$, and $\mathrm{M_{BH,C}}=0.5\times10^9\,\mathrm{M_\odot}$

ACKNOWLEDGEMENTS

MF acknowledges support by the Science and Technology Facilities Council [grant number ST/P000541/1] This project has received funding from the European Research Council (ERC) under the European Union's Horizon 2020 research and innovation programme (grant agreement No 757535) EPF acknowledges TTR® for the delightful discussions and the full support provided through the completation of this manuscript. This research made use of Astropy, a community–developed core Python package for Astronomy (Astropy Collaboration et al. 2013), of APLpy[4], an open–source plotting package for Python based on Matplotlib (Hunter 2007), and of IRAF[5]. We thank the members of the ENIGMA group[6] at the University of California, Santa Barbara (UCSB) for helpful discussions and comments on the manuscript.

REFERENCES

Aarseth S. J., Fall S. M., 1980, ApJ, 236, 43
Alexander D. M., Hickox R. C., 2012, NewAR, 56, 93
Aravena M., et al., 2008, A&A, 491, 173
Arrigoni Battaia F., Prochaska J. X., Hennawi J. F., Obreja A., Buck T., Cantalupo S., Dutton A. A., Macciò A. V., 2018, MNRAS, 473, 3907
Assef R. J., Stern D., Noirot G., Jun H. D., Cutri R. M., Eisenhardt P. R. M., 2018, ApJS, 234, 23
Astropy Collaboration, Robitaille, T. P., Tollerud, E. J., et al. 2013, A&A, 558, A33
Bañados E., Venemans B., Walter F., Kurk J., Overzier R., Ouchi M., 2013, ApJ, 773, 178
Bañados E., et al., 2017, arXiv, arXiv:1712.01860
Banerji M., Carilli C. L., Jones G., Wagg J., McMahon R. G., Hewett P. C., Alaghband-Zadeh S., Feruglio C., 2017, MNRAS, 465, 4390
Barvainis R., Alloin D., Guilloteau S., Antonucci R., 1998, ApJ, 492, L13
Behroozi P. S., Conroy C., Wechsler R. H., 2010, ApJ, 717, 379
Bouché N., et al., 2010, ApJ, 718, 1001
Bolatto A. D., Wolfire M., Leroy A. K., 2013, ARA&A, 51, 207
Bonning E. W., Shields G. A., Salviander S., 2007, ApJ, 666, L13
Carilli C. L., et al., 2002, AJ, 123, 1838
Carilli C. L., Walter F., 2013, ARA&A, 51, 105
Combes F., Young L. M., Bureau M., 2007, MNRAS, 377, 1795
Coppin K. E. K., et al., 2008, MNRAS, 389, 45
Coppin K. E. K., et al., 2010, MNRAS, 407, L103
Croom S. M., et al., 2005, MNRAS, 356, 415
Decarli R., Gavazzi G., Arosio I., Cortese L., Boselli A., Bonfanti C., Colpi M., 2007, MNRAS, 381, 136
Decarli R., Falomo R., Treves A., Labita M., Kotilainen J. K., Scarpa R., 2010, MNRAS, 402, 2453

[4] http://aplpy.github.io/
[5] IRAF (Tody 1986, 1993), is distributed by the National Optical Astronomy Observatories, which are operated by the Association of Universities for Research in Astronomy, Inc., under cooperative agreement with the National Science Foundation.
[6] http://enigma.physics.ucsb.edu/

Decarli R., et al., 2012, ApJ, 756, 150
Decarli R., et al., 2014, ApJ, 782, 78
Decarli R., et al., 2016, ApJ, 833, 69
Decarli R., et al., 2017, Natur, 545, 457
Decarli R., et al., 2018, arXiv, arXiv:1801.02641
Decarli et al. in preparation
Di Matteo T., Springel V., Hernquist L., 2005, Natur, 433, 604
Djorgovski S., 1991, ASPC, 21, 349
Djorgovski S. G., Courbin F., Meylan G., Sluse D., Thompson D., Mahabal A., Glikman E., 2007, ApJ, 662, L1
Dutton A. A., Macciò A. V., 2014, MNRAS, 441, 3359
Eftekharzadeh S., et al., 2015, MNRAS, 453, 2779
Eftekharzadeh S., Myers A. D., Hennawi J. F., Djorgovski S. G., Richards G. T., Mahabal A. A., Graham M. J., 2017, MNRAS, 468, 77
Fanidakis N., et al., 2013, MNRAS, 435, 679
Farina E. P., Falomo R., Treves A., 2011, MNRAS, 415, 3163
Farina E. P., Montuori C., Decarli R., Fumagalli M., 2013, MNRAS, 431, 1019
Farina E. P., et al., 2017, ApJ, 848, 78
Ferrarese L., Ford H., 2005, SSRv, 116, 523
Feruglio C., et al., 2014, A&A, 565, A91
Frayer D. T., Ivison R. J., Scoville N. Z., Yun M., Evans A. S., Smail I., Blain A. W., Kneib J.-P., 1998, ApJ, 506, L7
Foreman G., Volonteri M., Dotti M., 2009, ApJ, 693, 1554
García-Vergara C., Hennawi J.F., Barrientos L. F., Rix H.-W. 2017, ApJ, 848, 7
Goto T., Utsumi Y., Kikuta S., Miyazaki S., Shiki K., Hashimoto T., 2017, MNRAS, 470, L117
Girardi M., Giuricin G., Mardirossian F., Mezzetti M., Boschin W., 1998, ApJ, 505, 74
Green P. J., Myers A. D., Barkhouse W. A., Aldcroft T. L., Trichas M., Richards G. T., Ruiz Á., Hopkins P. F., 2011, ApJ, 743, 81
Guilloteau S., Omont A., Cox P., McMahon R. G., Petitjean P., 1999, A&A, 349, 363
Hainline L. J., Scoville N. Z., Yun M. S., Hawkins D. W., Frayer D. T., Isaak K. G., 2004, ApJ, 609, 61
Harris A. I., Baker A. J., Zonak S. G., Sharon C. E., Genzel R., Rauch K., Watts G., Creager R., 2010, ApJ, 723, 1139
Hennawi J. F., et al., 2006, AJ, 131, 1
Hennawi J. F., et al., 2010, ApJ, 719, 1672
Hennawi J. F., Prochaska J. X., Cantalupo S., Arrigoni-Battaia F., 2015, Sci, 348, 779
Hewett P. C., Wild V., 2010, MNRAS, 405, 2302
Hopkins P. F., Hernquist L., Cox T. J., Kereš D., 2008, ApJS, 175, 356-389
Hunter, J. D. 2007, Computing in Science and Engineering, 9, 90 8
Kayo I., Oguri M., 2012, MNRAS, 424, 1363
Kormendy J., Richstone D., 1995, ARA&A, 33, 581
Kormendy J., Ho L. C., 2013, ARA&A, 51, 511
Lacey C., Cole S., 1993, MNRAS, 262, 627
Laurent P., et al., 2017, JCAP, 7, 017
Limber D. N., Mathews W. G., 1960, ApJ, 132, 286
Lynden-Bell D., 1969, Natur, 223, 690
McGreer I.D., Eftekharzadeh S., Myers A.D., Fan X. 2016, AJ, 151, 61
Mazzucchelli C., Bañados E., Decarli R., Farina E. P., Venemans B. P., Walter F., Overzier R., 2017, ApJ, 834, 83
Martínez-Sansigre A., et al., 2009, ApJ, 706, 184
Merloni A., et al., 2010, ApJ, 708, 137
Moster B. P., Somerville R. S., Maulbetsch C., van den Bosch F. C., Macciò A. V., Naab T., Oser L., 2010, ApJ, 710, 903
Mortlock D. J., et al., 2011, Natur, 474, 616
Myers A. D., Brunner R. J., Nichol R. C., Richards G. T., Schneider D. P., Bahcall N. A., 2007, ApJ, 658, 85
Myers A. D., Richards G. T., Brunner R. J., Schneider D. P., Strand N. E., Hall P. B., Blomquist J. A., York D. G., 2008, ApJ, 678, 635-646
Navarro J. F., Frenk C. S., White S. D. M., 1997, ApJ, 490, 493
Neistein E., Dekel A., 2008, MNRAS, 383, 615
Niemi S.-M., Heinämäki P., Nurmi P., Saar E., 2010, MNRAS, 405, 477
Onoue M., et al., 2018, PASJ, 70, S31
Oke J. B., 1974, ApJS, 27, 21
Oke J. B., Gunn J. E., 1983, ApJ, 266, 713
Peng C. Y., Impey C. D., Ho L. C., Barton E. J., Rix H.-W., 2006, ApJ, 640, 114
Peng C. Y., Impey C. D., Rix H.-W., Kochanek C. S., Keeton C. R., Falco E. E., Lehár J., McLeod B. A., 2006, ApJ, 649, 616
Planck Collaboration, et al., 2014, A&A, 571, A16
Planesas P., Martin-Pintado J., Neri R., Colina L., 1999, Sci, 286, 2493
Popping G., van Kampen E., Decarli R., Spaans M., Somerville R. S., Trager S. C., 2016, MNRAS, 461, 93
Porciani C., Magliocchetti M., Norberg P., 2004, MNRAS, 355, 1010
Richards G. T., Vanden Berk D. E., Reichard T. A., Hall P. B., Schneider D. P., SubbaRao M., Thakar A. R., York D. G., 2002, AJ, 124, 1
Riechers D. A., Walter F., Carilli C. L., Lewis G. F., 2009, ApJ, 690, 463
Riechers D. A., et al., 2011, ApJ, 739, L32
Riechers D. A., 2011, ApJ, 730, 108
Rodríguez-Torres S. A., et al., 2017, MNRAS, 468, 728
Runnoe J. C., Brotherton M. S., Shang Z., 2012, MNRAS, 422, 478
Salpeter E. E., 1964, ApJ, 140, 796
Sandrinelli A., Falomo R., Treves A., Scarpa R., Uslenghi M., 2018, MNRAS, 474, 4925
Shankar F., Weinberg D. H., Miralda-Escudé J., 2009, ApJ, 690, 20
Shankar F., Weinberg D. H., Shen Y., 2010, MNRAS, 406, 1959
Shen Y., Hennawi J.F., Shankar F., Myers A.D., Strauss M.A., Djorgovski S.G., Fan X., Giocoli C., et al. 2010, ApJ, 719, 1693
Shen Y., McBride C.K., White M., Zheng Z., Myers A.D., Guo H., Kirkpatrick J.A., Padmanabhan N., et al. 2013, ApJ, 778, 98
Simpson J. M., et al., 2012, MNRAS, 426, 3201
Soltan A., 1982, MNRAS, 200, 115
Springel V., Di Matteo T., Hernquist L., 2005, MNRAS, 361, 776
Springel V., et al., 2005, Natur, 435, 629
Strazzullo V., et al., 2010, A&A, 524, A17
Tody D., 1986, SPIE, 627, 733
Tody D., 1993, ASPC, 52, 173
Tuan-Anh P., Hoai D. T., Nhung P. T., Diep P. N., Phuong N. T., Thao N. T., Darriulat P., 2017, MNRAS, 467, 3513
Venemans B. P., et al., 2017, ApJ, 845, 154
Vestergaard M., Osmer P. S., 2009, ApJ, 699, 800
Walter F., et al., 2003, Natur, 424, 406
Walter F., Carilli C., Bertoldi F., Menten K., Cox P., Lo K. Y., Fan X., Strauss M. A., 2004, ApJ, 615, L17
Walter F., et al., 2014, ApJ, 782, 79
Walter F., et al., 2016, ApJ, 833, 67
Wang R., et al., 2010, ApJ, 714, 699
Wang R., et al., 2011a, ApJ, 739, L34
Wang R., et al., 2011b, AJ, 142, 101
White S. D. M., Rees M. J., 1978, MNRAS, 183, 341
White M., et al., 2012, MNRAS, 424, 933
Willott C. J., Martínez-Sansigre A., Rawlings S., 2007, AJ, 133, 564

This paper has been typeset from a TEX/LATEX file prepared by the author.